



Deposited via The University of Sheffield.

White Rose Research Online URL for this paper:

<https://eprints.whiterose.ac.uk/id/eprint/237121/>

Version: Accepted Version

Article:

Zhu, W., De Gaetano, D., Sun, X. et al. (2025) Localized asymmetric behavior of common-mode current through bearing balls. IEEE Transactions on Energy Conversion. ISSN: 0885-8969

<https://doi.org/10.1109/tec.2025.3632796>

© 2025 The Authors. Except as otherwise noted, this author-accepted version of a journal article published in IEEE Transactions on Energy Conversion is made available via the University of Sheffield Research Publications and Copyright Policy under the terms of the Creative Commons Attribution 4.0 International License (CC-BY 4.0), which permits unrestricted use, distribution and reproduction in any medium, provided the original work is properly cited. To view a copy of this licence, visit <http://creativecommons.org/licenses/by/4.0/>

Reuse

This article is distributed under the terms of the Creative Commons Attribution (CC BY) licence. This licence allows you to distribute, remix, tweak, and build upon the work, even commercially, as long as you credit the authors for the original work. More information and the full terms of the licence here: <https://creativecommons.org/licenses/>

Takedown

If you consider content in White Rose Research Online to be in breach of UK law, please notify us by emailing eprints@whiterose.ac.uk including the URL of the record and the reason for the withdrawal request.

Localized Asymmetric Behavior of Common-Mode Current Through Bearing Balls

Wenjun Zhu, Daniele De Gaetano, *Member, IEEE*, Xiangyu Sun, *Student Member, IEEE*, Huanyu Li, *Student Member, IEEE*, Xiao Chen, *Senior Member, IEEE*, Antonio Griffo, and Geraint W. Jewell

Abstract--The high-frequency pulse width modulation in voltage source inverters generates common-mode voltage and current in inverter-fed electrical machine drive systems, leading to high-frequency bearing currents and potential bearing damage. Due to the enclosed structure of bearings and the distributed nature of bearing currents, accurate measurement remains challenging. This paper reviews existing measurement methods and identifies a previously unreported bearing current component caused by uneven potential distribution on the end-caps, termed the "end-cap bearing current." The "end-cap bearing current" occurs exclusively when the bearings are in a conducting state, which can happen during low-speed operation or bearing breakdown. Experimental results from a modified end-cap setup with multiple connection wires reveal asymmetric radial current flow through bearing balls, which is not captured by conventional single-wire measurement methods. A 3D finite element model and an enhanced circuit model are developed to illustrate the underlying mechanism. The study demonstrates that up to 25% of the high-frequency common-mode current in the end-cap may flow through the bearing balls under conductive conditions, highlighting the limitations of existing measurement techniques and the need for more accurate bearing current assessment.

Index Terms--AC machines, Ball bearings, High frequency, Voltage source inverters.

I. INTRODUCTION

THE voltage source inverter-fed AC machine drive systems are potentially at risk of high frequency bearing currents which can lead to bearing aging or even failure. The common-mode voltage and common-mode current are considered to be the sources of these high frequency bearing currents [1, 2]. Despite various modeling and calculation techniques proposed in literature, the experimental measurement setup for bearing currents is not well documented. Due to the enclosed structure of the bearings and electrical machine and the complex distribution of bearing currents, accurately measuring bearing currents is challenging.

This paper first introduces the existing measurement methods in literature in Section II. The most commonly used arrangement uses an insulation layer between the bearings and

the conductive end-cap/frame of the machine, and a single conducting jumper wire between the end-cap and the bearing which conducts the bearing currents and allow their direct measurement [3, 4]. This arrangement forces the bearing currents, which would naturally be distributed on the circumference of the bearing, to flow through a single wire, altering its natural path. In this case an intuitive question arises: will the asymmetric modification have any effect on the bearing currents? To answer this question, it may be intuitive to add multiple connection wires between the end-cap and the bearing surfaces, arranged symmetrically, to provide a more representative method for the bearing currents to flow in the radial direction. In this paper, experiments were conducted to identify the most accurate arrangement for bearing current measurement. The experiments and analyses demonstrate that multiple connection wires result in a significantly different pattern for the flow of bearing currents. The detailed experimental setup and measured results can be found in Section III. In Section IV, the measured results are explained, and a new bearing current component due to uneven potential distribution on the end-cap, named "end-cap bearing current", is identified. To the best of the authors' knowledge, this bearing current component has not been reported before. A three-dimensional (3D) finite element analysis (FEA) model and a circuit model are developed to illustrate the mechanism of the "end-cap bearing current." Section V discusses the effects of the end-cap bearing current and the mitigation strategies.

II. EXISTING BEARING CURRENTS MEASUREMENT METHODS

The term "bearing currents" in this context specifically refers to the currents that flow through the bearing balls, potentially causing damages to the bearing races, such as pitting, frosting and fluting [5, 6]. Depending on whether any additional modifications are necessary for the machine, the measurement methods can be categorized as either intrusive or non-intrusive.

The non-intrusive measurement method involves the use of a radio frequency (RF) antenna, as reported in [7], to detect the occurrence of electrical discharge machining (EDM) bearing currents, as illustrated in Fig. 1. Alternatively, a magnetic near-

This work was supported by U.K. EPSRC through research award EP/W015838/1. For the purpose of open access, the authors have applied a Creative Commons Attribution (CC BY) license to any Author Accepted Manuscript version arising.

Wenjun Zhu is with the School of Robotics, Xi'an Jiaotong-Liverpool University, Suzhou, 215412 China (e-mail: wenjun.zhu02@xjtlu.edu.cn).

D. De Gaetano is with Advanced Manufacturing Research Centre, University of Sheffield, Sheffield, S60 5TZ UK (email: d.degaetano@sheffield.ac.uk)

Xiangyu Sun is with the School of Electrical and Electronic Engineering, University of Sheffield, Sheffield, S1 4DT UK (email: xiangyu.sun@sheffield.ac.uk)

Huanyu Li is with the School of Electrical and Electronic Engineering, University of Sheffield, Sheffield, S1 4DT UK (email: hli209@sheffield.ac.uk)

Xiao Chen is with the School of Electrical and Electronic Engineering, University of Sheffield, Sheffield, S1 4DT UK (email: xiao.chen@sheffield.ac.uk)

Antonio Griffo is with the School of Electrical and Electronic Engineering, University of Sheffield, Sheffield, S1 4DT UK (email: a.griffo@sheffield.ac.uk)

Geraint W. Jewell is with the School of Electrical and Electronic Engineering, University of Sheffield, Sheffield, S1 4DT UK (email: g.jewell@sheffield.ac.uk)

field probe has been designed and evaluated in [8]. It is important to consider the bandwidth and sensitivity to RF noise of these non-intrusive measurement methods. Measurement in inverter-fed machines which produce significant RF noise is particularly problematic. Additionally, it has been demonstrated that the RF-based method is also suitable for capturing high-frequency circulating bearing currents [9]. This approach does not require any additional modifications to the machine but is sensitive to electromagnetic interference.

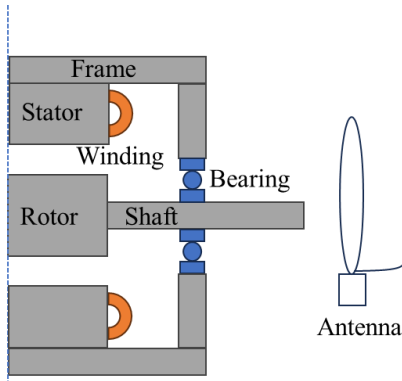


Fig. 1. RF antenna set up for EDM bearing current measurements.

A measurement approach with the addition of external bearing (Fig. 2) was proposed in [10]. In this method, the stator frame needs to be electrically isolated from the existing bearings through an additional insulation layer. The external bearings conduct the electrical currents through grounded cables connected to their outer races while the machine-mounted bearings only support the mechanical load. The challenge in this approach is that the external bearings may behave differently in terms of electrical characteristics since there is no mechanical load on the external bearings. Hence, they may not accurately reflect the actual bearing currents of the original bearings.

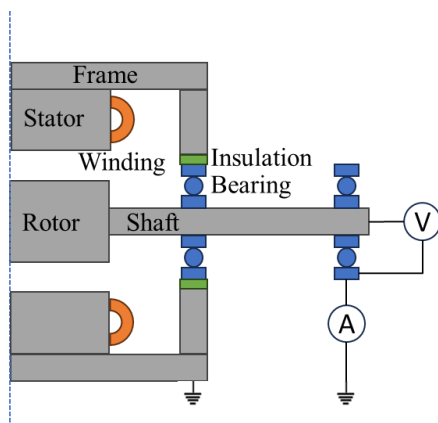


Fig. 2. External bearings set up for bearing current measurements.

As shown in Fig. 3, the shaft current can be measured using Rogowski coils installed on the shaft [3, 11]. The output leads of the Rogowski coils can be routed through a hole in the end-caps, or alternatively, the data can be transmitted using wireless communication. The Rogowski coil method does not alter the

bearing current path of the machine, but embedding Rogowski coils is often challenging due to the limited space within the electrical machine. Note that the current measured using this method is the shaft current which may represent only part of the bearing currents, such as the circulating bearing current component. For example, rotor ground current is not enclosed by the Rogowski coils and cannot be captured using this method.

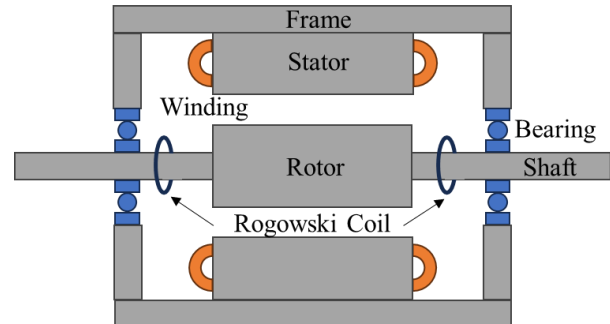


Fig. 3. Rogowski coils set up for shaft current measurements.

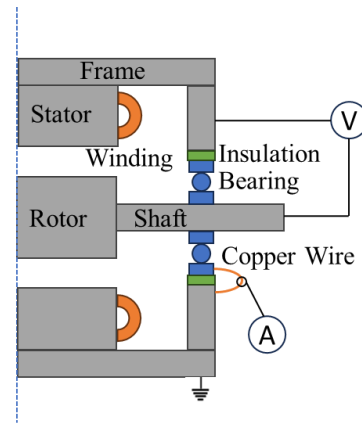


Fig. 4. Insulated bearing and one jump wire set up for bearing current measurements.

The insulated bearing with one jumper wire, depicted in Fig. 4, is the most commonly used method in literature [12-14]. The jumper wire introduced additional resistance and impedance in parallel with the capacitance of the insulation layer. Therefore, correction must be applied when calculating the real bearing current from the measurement results [15]. However, using only one wire forces the currents to flow through that specific wire, resulting in an asymmetric distribution of currents along the circumferential direction. This asymmetry contradicts the 360° distributed bearing current phenomenon on the end-caps of the unmodified machine. Table I summarizes and compares different measurement methods, along with the corresponding literature in which they are used.

TABLE I
Comparison of Measurement Methods

Measurement Method	Literature	Advantages	Disadvantages
RF antenna	[7],[9],[16],[17],[18]	<ul style="list-style-type: none"> No machine modification required. Capable of detecting EDM currents and high- 	<ul style="list-style-type: none"> Highly sensitive to EMI. Typically used for qualitative detection rather than accurate

		frequency circulating currents.	quantification of current amplitude. • Requires high-bandwidth and high-sensitivity equipment.
External bearing	[10]	• Separates the measurement bearing from the operational ones, avoiding interference with the machine's mechanical function.	• The external bearing is unloaded mechanically. • Requires structural modification of the machine.
Embedded Rogowski coils	[3],[11],[19],[20]	• Does not alter the natural path of the bearing currents. • Suitable for measuring high-frequency currents.	• Limited installation space makes embedding the coil inside a machine challenging. • Only captures current through the shaft.
Insulated bearing with one jumper wire	[12],[13],[14],[15],[21],[22],[23],[24]	• Relatively simple to implement and is the most prevalent method found in literature. • Provides a direct measurement of current at the bearing location.	• Severely distorts the natural current distribution. • Introduces additional parasitic impedance.

III. MULTIPLE CONNECTION WIRES SET-UP AND RESULTS

In order to evaluate the asymmetry in the current distribution, an insulation layer was introduced in the middle of the end-cap, as shown in Fig. 5. To allow for multiple connections, six sets of bolts were positioned with a 60° angular space, providing flexibility in establishing multiple connections.

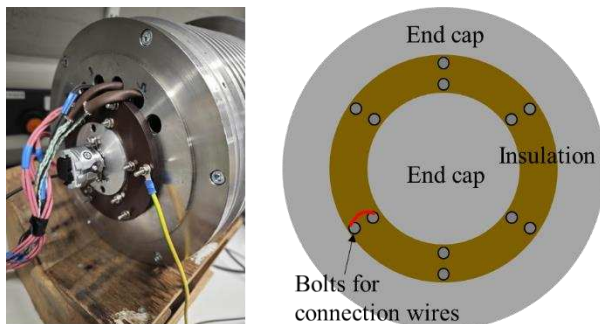


Fig. 5. Modified end-cap and its schematic.

The experimental setup, illustrated in Fig. 6, consists of a Nidec Unidrive M700 inverter and a 10kW permanent magnet machine. Two Rogowski coils (PEMCMC015) are embedded in the machine around the shaft, one on the drive end (DE) and the other on the non-drive end (NDE), to measure the shaft current. High bandwidth current probes (Tektronix - probe: TCP305A; Tektronix - amplifier: TCPA 300) are positioned on the wire branches, and an additional Rogowski coil is placed on the ground wire to measure the ground current.

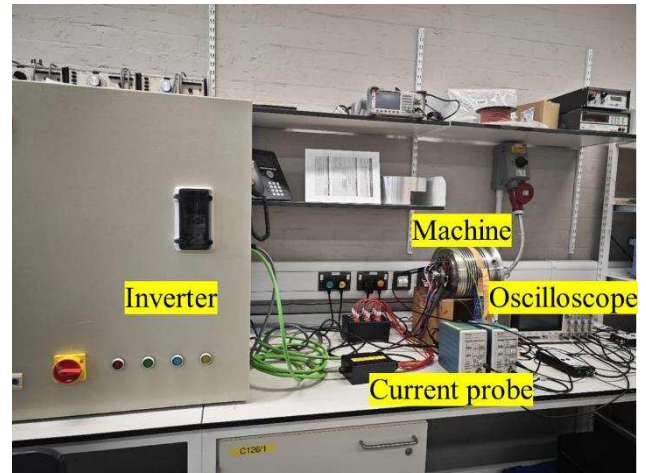


Fig. 6. Test rig of the bearing current measurements at no-load conditions.

Using a single wire branch connection, the test was conducted at a switching frequency of 12 kHz and speeds of 5 rpm and 200 rpm, as depicted in Fig. 7. At 5 rpm, the bearings exhibit a conductive behavior. This suggests that at this low rotational speed, there is not enough relative motion between the bearing components to establish a sufficient lubricant oil film. In other words, the lubrication mechanism is insufficient to prevent metal-to-metal contact, which can result in electrical conducting behavior due to the direct contact of metal balls with their races. As the rotational speed increases to 200 rpm, the bearings demonstrate capacitive behaviors. This change in behavior indicates that a lubricant oil film is now effectively formed and hence separates the metal balls from their races. The presence of this film insulates the bearing components, reducing electrical conduction and leading to a capacitive behavior [25]. The measured currents at 5 rpm and 200 rpm are illustrated in Fig. 8 and Fig. 10, respectively. Correspondingly, the Fast Fourier Transform was applied to show the frequency spectrum of the measured currents, as shown in Fig. 9 and Fig. 11.

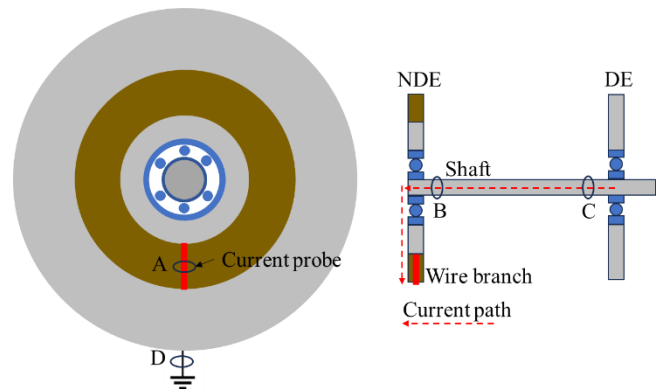


Fig. 7. One wire branch connection with current path illustration.

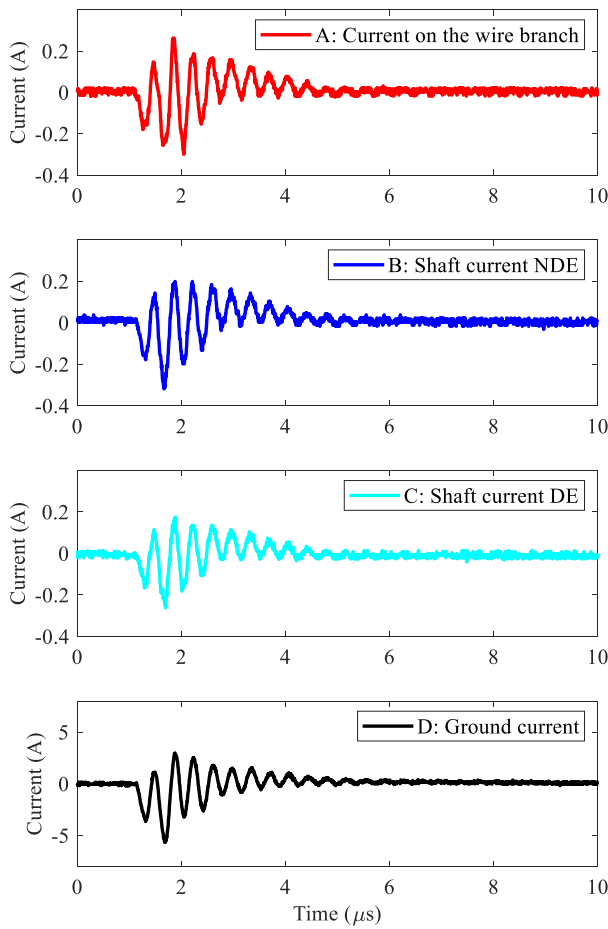


Fig. 8. Measured currents with one wire branch connection at 5 rpm, no-load condition.

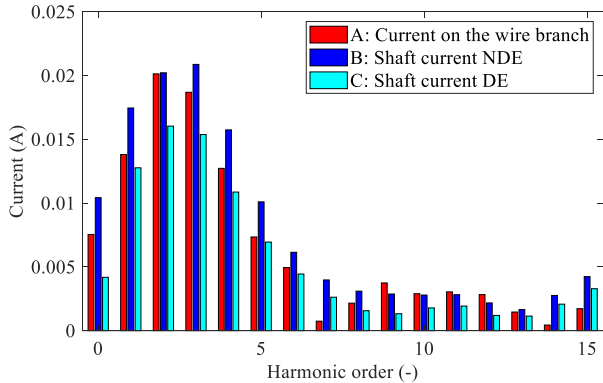


Fig. 9. Frequency spectrum analysis of the measured currents with one wire branch connection at 5 rpm, no-load condition.

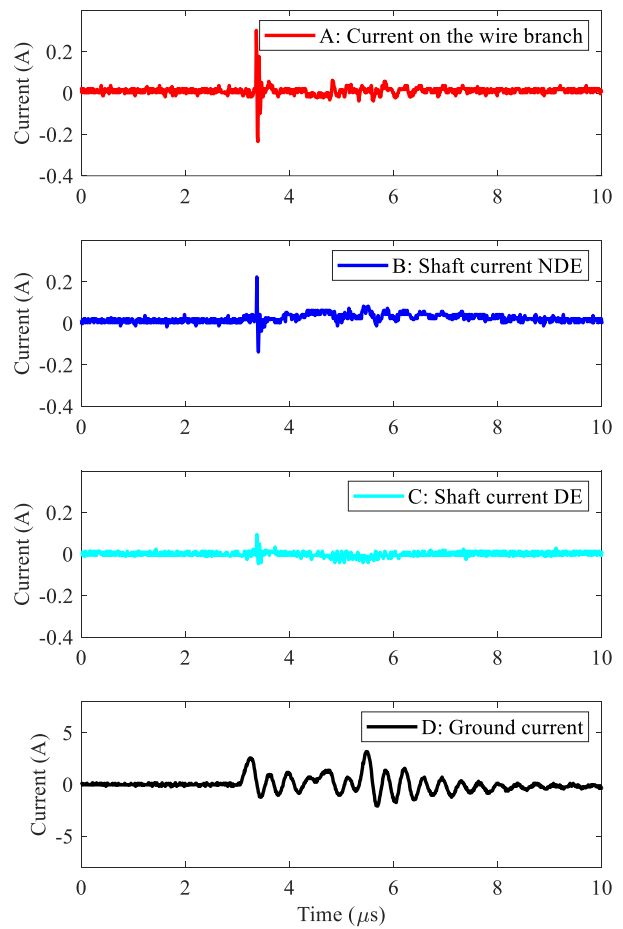


Fig. 10. Measured currents with one wire branch connection at 200 rpm, no-load condition.

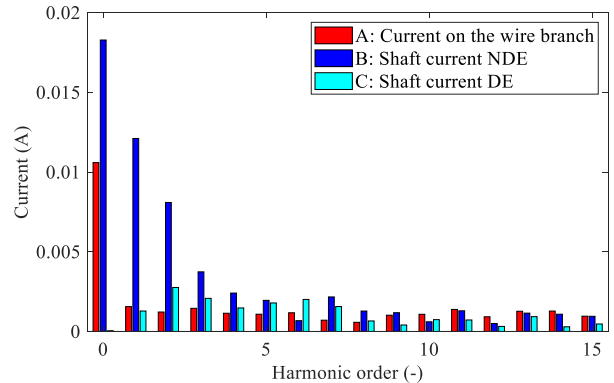


Fig. 11. Frequency spectrum analysis of the measured currents with one wire branch connection at 200 rpm, no-load condition.

The current in the wire branch is measured using a high-bandwidth current probe. The shaft currents at the NDE and DE are measured by two embedded Rogowski coils, positioned at the respective ends of the shaft. Ground current is measured by a current probe clamped onto the grounding wire connected to the frame. The measured current begins to oscillate, synchronized with the switching actions of the inverter.

From Figs. 8-11, it can be seen that the current flowing in the branch nearly equals the current flowing in the shaft, which is not a surprise as this single branch is the only path for current to flow. In the case of the 200 rpm condition, the shaft current

is attenuated due to the larger bearing capacitance, while occasional spikes in the current waveform indicate the occurrence of EDM bearing currents.

When two wire branches connecting the bearing to the end-cap are introduced (as shown in Fig. 12), one might initially assume that the two branches would evenly share the shaft current if symmetry is ensured. However, this assumption contradicts the experimental findings. The measured currents are illustrated in Fig. 13 and Fig. 15, together with the frequency spectrum in Fig. 14 and Fig. 16. At 5 rpm (Fig. 13), the current on wire branch 1 equals the sum of the current on wire branch 2 and the shaft current, which aligns with the concept of a “T” junction of current path illustrated in Fig. 12. At 200 rpm (Fig. 15), the shaft current is significantly reduced due to the formation of lubrication film. The currents flowing in the branches are greater than the current flowing in the shaft in terms of magnitude. This indicates that the high frequency current flows into one branch (through current probe 2 in Fig. 12), and then joined with the shaft current before flowing out through the other branch (through current probe 1 in Fig. 12). As a result, the bearing current is not fully captured by the Rogowski coil installed on the shaft. The currents in the branches are flowing in the radial direction in the end-cap due to asymmetric ground as shown in Fig. 12 because all the current will finally reach the ground point on the frame.

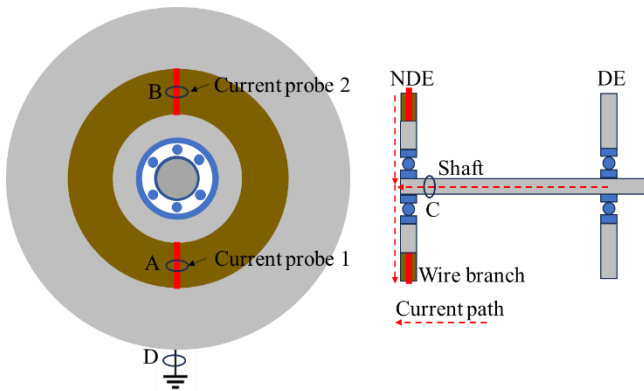


Fig. 12. Schematic of two wire branches connection with current path illustration.

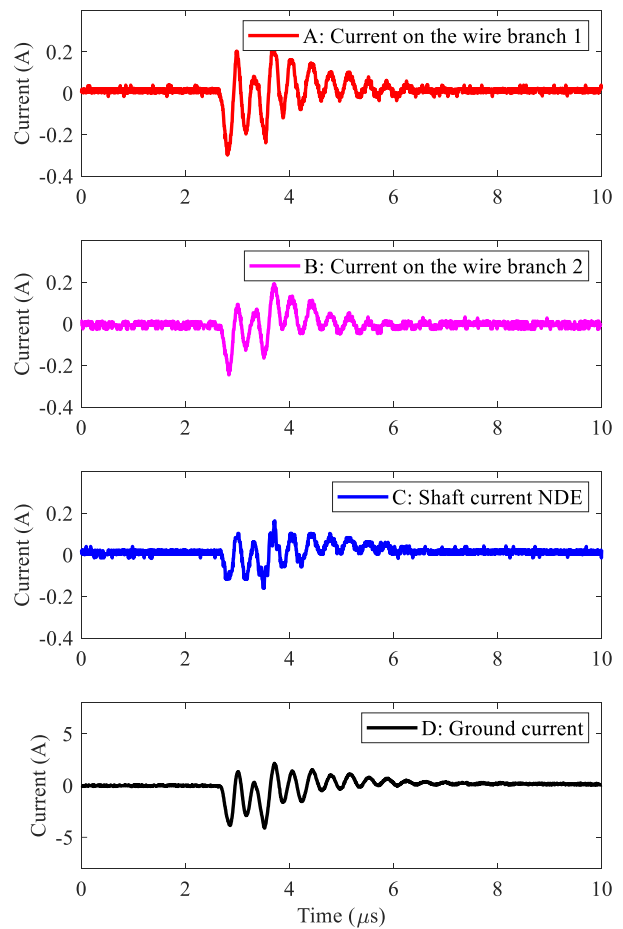


Fig. 13. Measured currents with two wire branches connection at 5 rpm, no-load condition.

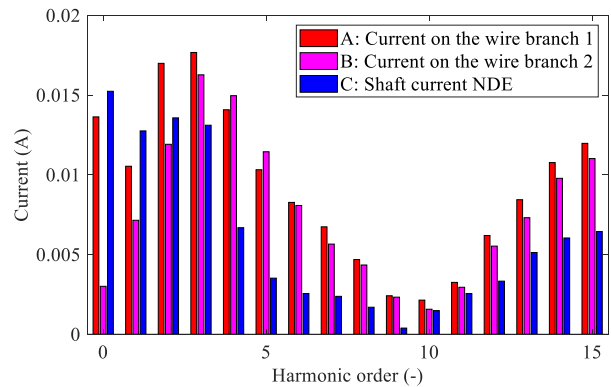


Fig. 14. Frequency spectrum analysis of the measured currents with two wire branches connection at 5 rpm, no-load condition.

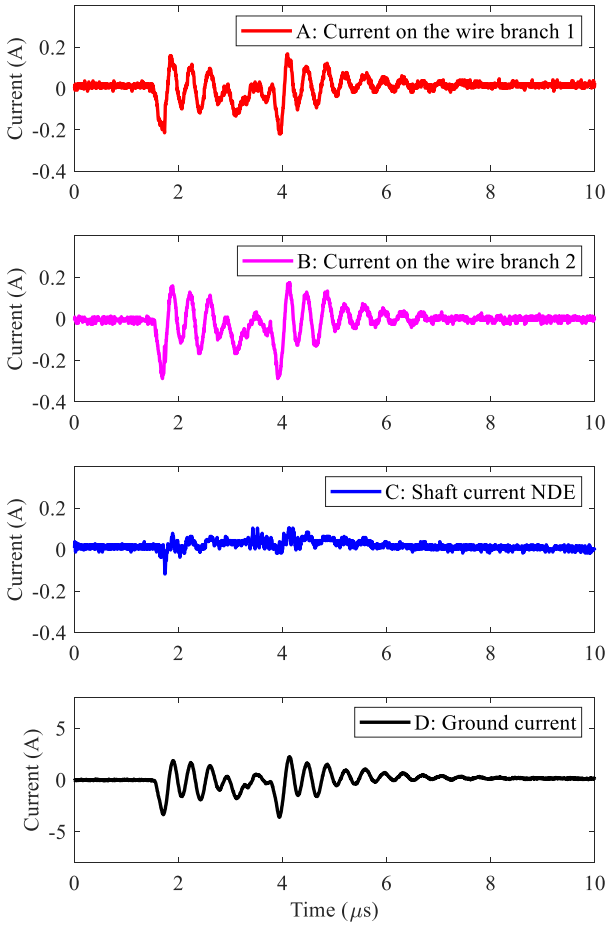


Fig. 15. Measured currents with two wire branches connection at 200 rpm, no-load condition.

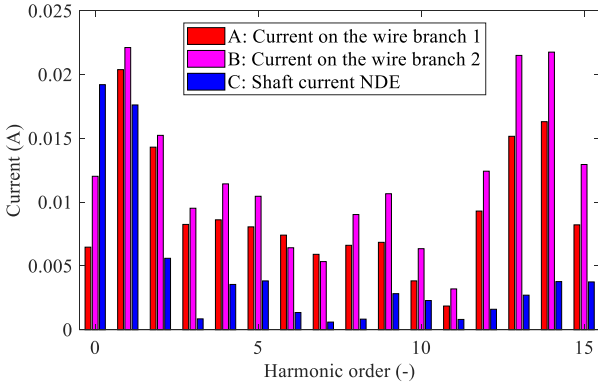


Fig. 16. Frequency spectrum analysis of the measured currents with two wire branches connection at 200 rpm, no-load condition.

Table II summarizes the peak values of the experiment measured current of different set ups. From the experimental evidence, the different behaviors exist for the common-mode current in the one branch set up and the two branches set up. With one branch set up, the natural current path is disrupted, forcing all current through a single wire in the “L” shaped junction as illustrated in Fig. 7. With two branches set up, the current can flow in the radial direction through the end-cap, with a “T” junction as illustrated in Fig. 12, which means some current came from one branch and flow through the other branch, without entering the shaft. More detailed explanation

will be provided in Section IV.

TABLE II
Peak Value of Measured Currents

Peak value (A)	Fig. 8	Fig. 10	Fig. 13	Fig. 15
Current on the wire branch 1	0.30	0.30	0.30	0.22
Current on the wire branch 2	-	-	0.25	0.29
Shaft current NDE	0.32	0.22	0.16	0.12
Shaft current DE	0.26	0.09	-	-
Ground current	5.67	3.18	4.11	3.60

IV. END-CAP BEARING CURRENT

A. Explanation and Mechanisms

In the original unmodified end-caps (as depicted in Fig. 17), the bearing balls contact both the inner race and outer race of the bearing at low speeds when the lubrication film has not been formed, leading to a conductive behavior for the bearing. Consequently, the effects of the bearing balls on conducting currents are similar to those of the wire branches.

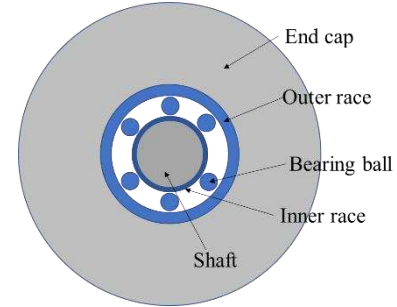


Fig. 17. Schematic of the original unmodified end-caps.

Based on the concept that the bearing balls resemble wire branches from an electrical perspective at low speeds, the modification made to the end-cap can be conceptualized as having two layers of current-conducting structures. The structure can be depicted as an inner ring and an outer ring with multiple connections in the radial direction, as shown in Fig. 18. Additionally, Fig. 19 illustrates the two layers of current-conducting structures in the modified end-cap. The outer layer features insulation and wire branches, while the inner layer comprises the actual bearing with races and balls.

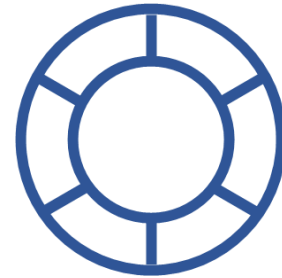


Fig. 18. Equivalent structure of bearing in terms of conducting current at low speeds when the lubrication film has not been formed.

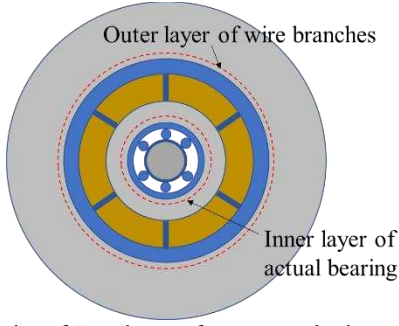


Fig. 19. Illustration of "two layers of current-conducting structures" in the modified end-caps.

Then the actual bearing and wire branches present very similar structures for conducting current. The behavior observed in the wire branches can serve as a qualitative representation of what occurs in the balls within the actual bearing. Therefore, the phenomena observed in the wire branches can provide valuable insights into the qualitative understanding of the behavior of the balls in the bearing.

In ball bearings, the balls are usually constrained with a bearing cage, as shown in Fig. 20 (a). The bearing cage could be conducted with multiple balls. However, as shown in Fig. 20 (b), the bearing cage can be considered as another layer of the typical structure in Fig. 18. The bearing cage only provides additional current path between the balls and will not affect the fact that some current flows through the balls.

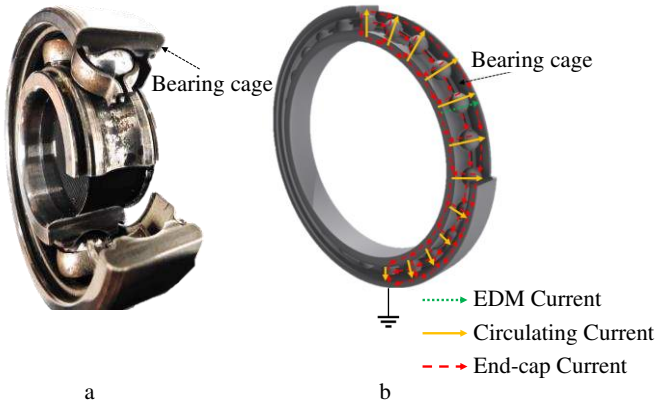


Fig. 20. Bearing cage: (a) Photo of bearing cage; (b) illustration of structure of bearing cage and current path of different bearing current components.

Considering that the currents in the two branches have greater magnitude than the current in the shaft, as shown in Fig. 13 and Fig. 15, there exists a current component which flows from one branch to the other without going through the shaft. Hence, it is a reasonable inference that in the original unmodified machine, there exists one current component flowing from one bearing ball to another ball without going through the shaft. This current component flows through the following path: end-cap \rightarrow bearing balls \rightarrow bearing cage \rightarrow bearing balls \rightarrow end-cap \rightarrow ground point, as shown in Fig. 20 (b). And this current does not go through the rotor/shaft to the ground, and thus it is fundamentally different from the rotor ground current reported in literature. This current component which has not been previously reported, is termed "end-cap bearing currents". In addition to the four recognized types of

bearing currents documented in literature [13, 26], the identification of this bearing current component is presented in Fig. 21 [15].

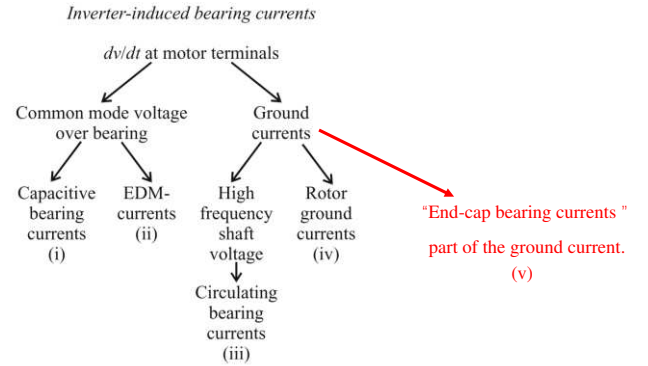


Fig. 21. Classification of bearing currents in inverter-fed electrical machines [15].

Table III summarizes the mechanisms of different types of bearing currents, along with representative literature on their modelling and analysis.

TABLE III
Different Types of Bearing Currents

Bearing current components	Mechanism	Literature
(i) Capacitive bearing currents	A high-frequency displacement current that flows through the parasitic capacitance formed by the lubricating film between the bearing balls and races.	[27],[28],
(ii) EDM currents	A transient, high-current discharge that occurs when the voltage across the bearing lubricating film exceeds its dielectric breakdown threshold.	[6],[27], [28], [29], [30],[31], [32],[33]
(iii) Circulating bearing currents	A circulating current that flows in a loop comprising the shaft, both drive-end and non-drive-end bearings, and the motor frame. It is induced by a high-frequency common-mode magnetic flux encircling the motor shaft.	[21],[33], [34],[35], [36],[37]
(iv) Rotor ground currents	The current that flows from the rotor, through a bearing, to the grounded motor frame. This occurs when the rotor has a potential relative to the ground, providing a path for the common-mode current to discharge to earth.	[38],[39],[40]
(v) End-cap bearing currents	A high-frequency current that flows radially through bearing balls from one point on the end-cap to another, bypassing the shaft. It is driven by an uneven potential distribution along the end-cap's circumference.	This paper

This bearing current component does not always exist, and it is dependent on certain conditions. It is present when both of the following conditions are satisfied:

1) The bearing balls provides a conducting path of outer race-balls-inner race-balls. This situation can occur at low speeds when the lubrication film has not yet formed or in the event of bearing breakdown. Detailed explanation is presented in Section IV.C.

2) An uneven potential distribution along the circumferential

direction on the end-cap leads to currents flowing from high to low potential. This uneven potential arises for several reasons: first, asymmetric grounding, such as grounding at a single point on the frame; second, the time-varying voltage of different coils positioned in different slots; and third, the asymmetric contact between bearing balls and races that happens randomly.

B. FEA Model

In order to gain a more comprehensive understanding of the end-cap bearing current, a simplified 3D FEA model was constructed using Altair Flux, as illustrated in Fig. 22. The model provides a simplified representation of the machine structure including the shaft, stator core, frame, and six branches on both sides of the end-caps. This model provides a clearer insight into the current distribution and behavior within the machine.

By applying an AC current excitation to the stator core and allowing it to flow out at the ground point to represent the common-mode current, the current density distribution within the model can be visualized, as shown in Fig. 23. The uneven distribution of currents among various branches is apparent. Table IV provides a list of Joule losses at the six branches, normalized to the highest Joule loss within those six branches. Since the materials and geometries of each branch are identical, the Joule losses can serve as indicators of the uneven current distribution among branches. Moreover, at this time instant, four of the branches carry currents from the frame to the rotor, while the remaining two branches carry currents from the rotor to the frame. Similarly, within the bearings, it can be imagined that a similar uneven current load distribution exists among the bearing balls. The currents flow into the inner race through certain balls and then flow out through other balls, eventually joining the ground connection.

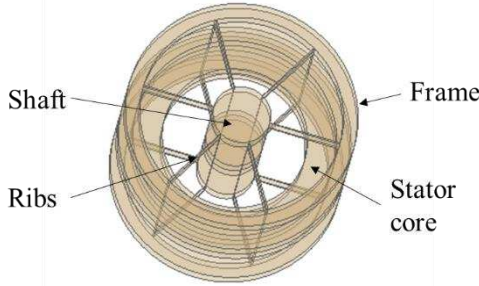


Fig. 22. Simplified 3D model for bearing current distribution investigation.

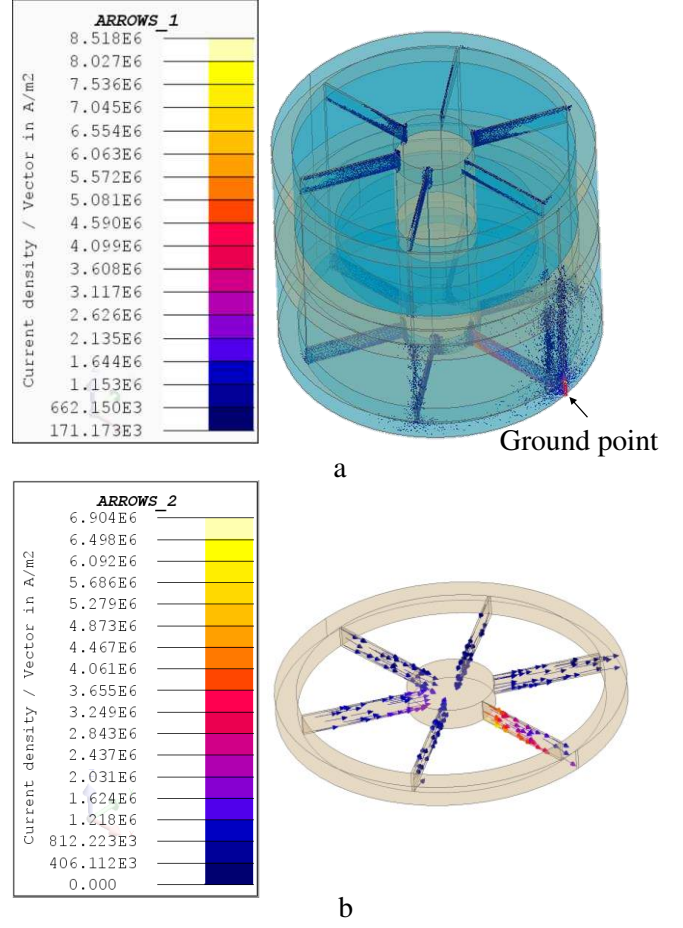


Fig. 23. Current density distribution at 1MHz. (a) whole model; (b) the bottom end-cap with branches.

TABLE IV
Joule Losses at 6 Branches

Branch	Joule Losses (per unit)
1st	1
2nd	0.119
3rd	0.058
4th	0.042
5th	0.024
6th	0.017

C. Circuit Model

The conventional common-mode circuit [14, 41, 42] (Fig. 24) in an electrical machine for EDM bearing current analysis contains the parasitic capacitive couplings of the winding, the rotor and the frame. In Fig. 24, V_{com} is the common-mode voltage generated by the inverter, C_{wf} is the winding to frame capacitance, C_{wr} is the winding to rotor capacitance, and C_{rf} is the rotor to frame capacitance. The bearings are simply represented by a capacitance (C_{b1} for the NDE bearing and C_{b2} for the DE bearing) and a resistance with a switch to model the bearing breakdown.

However, as the bearings normally contain multiple balls or cylinder rollers, the simplified circuit cannot fully reflect the structure of the bearings. Hence, this paper also proposes a new common-mode circuit model to account for the effect of the multiple balls of bearings, shown in Fig. 25. In Fig. 25, C'_{b1} and

C''_{b1} reflect the multiple capacitive connections between the inner race and outer race of the NDE bearing, and C'_{b2} and C''_{b2} are those capacitances corresponding to the DE bearing. Z_{cm} is the impedance of the common-mode current path in the end-cap.

By using two capacitors to model one bearing, it creates multiple connections from the frame to the rotor, establishing an alternative current pathway without entering the rotor. When the bearings are resistive conducting, the bearings provide a parallel path for the ground current, as illustrated in Fig. 25, which explains the end-cap bearing current is a current divider of the common-mode current.

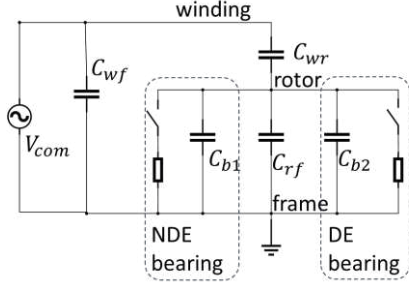


Fig. 24. Conventional common-mode circuit in an electrical machine. [14, 41, 42]

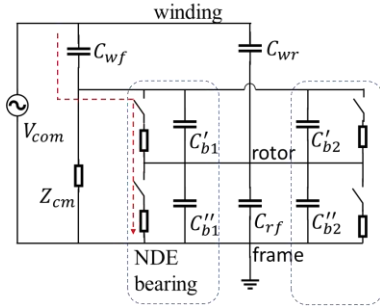


Fig. 25. Proposed common-mode circuit in an electrical machine.

During high-speed operation, a lubricating oil film forms between the race and balls in the bearings. As a result, the bearing behaviour resembles that of a capacitor. However, with a capacitor, it is anticipated that the current would flow along the outer race of the bearing, as it provides a low impedance path, as depicted in Fig. 26 (a). This is the case unless the bearing experiences a breakdown and reverts to a conducting state due to the presence of EDM currents. In the event of bearing breakdown or during low-speed operation, the bearing primarily behaves as a resistor. The impedance of the bearing in conducting state is denoted as Z_{bc} . With Z_{cm} in parallel connection, a current divider flows through the bearing balls, as depicted in Fig. 26 (b).

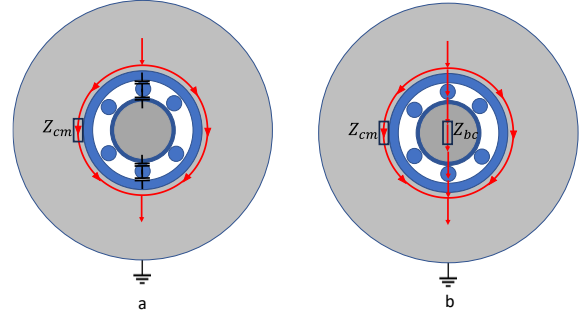


Fig. 26. Illustration of current paths in the end-cap at various conditions. (a) current bypasses the bearing balls at high-speed operations without breakdown of lubrication film; (b) current flows through the bearing balls at low-speed operations or high-speed operations with breakdown of lubrication film.

To have a sense of the current divider ratio, the standalone end-cap with the bearing seated in the chamber was measured using the impedance analyzer Hioki IM3570, as shown in Fig. 27. Two bearings were tested: the SKF 6004-2RSLTN9/HC5C3WT and the SKF 6004-2RSH. These bearings are identical except for the type of balls they use—SKF 6004-2RSH contains metal balls, whereas SKF 6004-2RSLTN9/HC5C3WT uses ceramic balls. In a static condition, when using metal balls, the measured impedance is Z_{bc} in parallel with Z_{cm} . However, with the hybrid ceramic bearing, the measured impedance is Z_{cm} alone. Then Z_{bc} can be calculated using the parallel configuration. The test results are presented in Table V. For example, at 700 kHz, Z_{bc} is 3.29 Ω , and Z_{cm} is 1.07 Ω . This means that approximately 25% of the total current flows through Z_{bc} , passing through the balls.

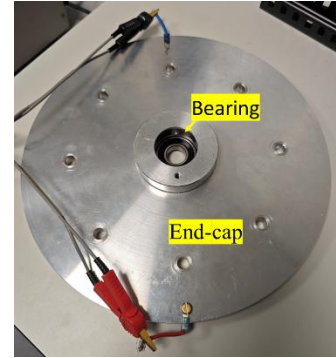


Fig. 27. Impedance measurement set up.

TABLE V
End-cap Impedance Results

Frequency (Hz)	$Z_{cm} // Z_{bc}^*$		Z_{cm}^{**}		Z_{bc}^{***}	
	Z (Ω)	PH ($^\circ$)	Z (Ω)	PH ($^\circ$)	Z (Ω)	PH ($^\circ$)
100k	0.12	87.8	0.16	88.5	0.50	85.5
200k	0.23	88.5	0.31	89.0	0.96	86.8
300k	0.35	88.9	0.46	89.3	1.44	87.5
400k	0.46	89.1	0.61	89.5	1.91	88.0
500k	0.58	89.3	0.77	89.6	2.37	88.3
600k	0.69	89.5	0.92	89.8	2.83	88.7
700k	0.81	89.6	1.07	89.9	3.29	88.9

*: Measured with SKF 6004-2RSH.

** : Measured with SKF 6004-2RSLTN9/HC5C3WT.

***: Calculated.

V. DISCUSSION

A. Impact of the "End-cap Bearing Currents"

The impact of the "end-cap bearing current" on bearing health is conditional and can be analyzed through three operational scenarios:

1) High-Speed Operation (Capacitive State): When a full lubricant film is present, the current bypasses the balls via the lower-impedance outer race. In this state, the "end-cap bearing current" is negligible and poses no direct threat.

2) Low-Speed Operation (Resistive State): During metal-to-metal contact, this current flows through the balls. The effects are strongly depended on the current density. With localized high current density at contact points, it is possible to result in micro-welding, electrical pitting, and gradual surface degradation over time, acting as a precursor to more severe failure.

3) Bearing Breakdown (EDM Events): This is the most critical scenario. During a dielectric breakdown, the "end-cap bearing current" can superimpose onto the EDM discharge current. This superposition increases the total charge and energy dissipated at the discharge point, amplifying the damage (e.g., creating larger craters) and potentially accelerating the formation of fluting.

However, the discussion above is qualitative, which calls into question the established understanding of the harmful effects of the "end-cap" bearing currents. Further study is needed to quantify this risk.

B. Mitigation Strategies

The identification of the "end-cap bearing current" further underscores the complexity of current paths and the importance of effective mitigation.

Several practical strategies exist to suppress the common-mode voltage and currents that are the root cause of all bearing current components, including the "end-cap bearing current", which is regarded as a current divider of the common-mode current. Installing a common-mode choke or dv/dt filters at the inverter output to slow down the voltage rise times of the PWM pulses. This reduces the amplitude of the high-frequency common-mode currents generated, thereby diminishing all related bearing current phenomena.

Apart from direct mitigating the common-mode current from the source, localized protection on the bearings can be adopted, such as bearing insulation to block the pathway for bearing currents. Replacing standard steel-ball bearings with hybrid bearings (steel races, ceramic balls) significantly increases the impedance through the balls (Z_{bc}). Ceramic balls present a much higher impedance path. This effectively diverts the common-mode current away from the balls, mitigating both the "end-cap bearing current" and the damaging EDM currents that flow through the rolling elements.

The selection of an appropriate mitigation strategy depends on the specific drive system, operational profile, and cost considerations.

VI. CONCLUSION

This paper has identified and experimentally validated a new

bearing current component, referred to as the "end-cap bearing current," which arises from asymmetrical potential distribution along the circumferential direction of the end-cap. Through a modified end-cap setup with multiple connection wires, it was demonstrated that common-mode currents can flow radially through bearing balls without passing through the shaft—a behavior not captured by traditional single-wire measurement methods. The proposed 3D FEA and circuit models provide insight into the mechanism of this current component, showing that it acts as a current divider of the common-mode current and can constitute a significant portion (up to ~25%) of the total end-cap current under conductive bearing conditions.

The "end-cap" bearing current is only a concern when the bearing is in a conductive state. This occurs either during low-speed operation, which permits metal-to-metal contact, or during an EDM discharge event, where the dielectric breakdown temporarily creates a conductive path. However, if a lubricant film exists, acting as a capacitor, this current will bypass the bearing balls and instead flow through the outer race of the bearings.

The findings underscore the limitations of existing bearing current measurement methods, particularly the single-wire approach, which disrupts the natural current path and fails to capture the full extent of bearing currents. Future work should focus on quantifying the risk associated with this current component and developing non-intrusive measurement techniques capable of accurately assessing all bearing current types in operating machines.

VII. REFERENCES

- [1] W. Zhu, D. De Gaetano, X. Chen, G. W. Jewell, and Y. Hu, "A Review of Modeling and Mitigation Techniques for Bearing Currents in Electrical Machines With Variable-Frequency Drives," *IEEE Access*, vol. 10, pp. 125279–125297, 2022.
- [2] K. B. Tawfiq, M. Güleç, and P. Sergeant, "Bearing Current and Shaft Voltage in Electrical Machines: A Comprehensive Research Review," *Machines*, vol. 11, no. 5, p. 550, 2023.
- [3] R. Ong, J. H. Dymond, and R. D. Findlay, "Comparison of techniques for measurement of shaft currents in rotating machines," *IEEE Transactions on Energy Conversion*, vol. 12, no. 4, pp. 363–367, 1997.
- [4] A. Kempski, R. Strzelecki, R. Smolenski, and Z. Fedyczak, "Bearing current path and pulse rate in PWM-inverter-fed induction," in *2001 IEEE 32nd Annual Power Electronics Specialists Conference (IEEE Cat. No. 01CH37230)*, 2001.
- [5] D. Busse, J. Erdman, R. J. Kerkman, D. Schlegel, and G. Skibinski, "Bearing currents and their relationship to PWM drives," *IEEE Transactions on Power Electronics*, vol. 12, no. 2, pp. 243–252, 1997.
- [6] D. F. Busse, J. M. Erdman, R. J. Kerkman, D. W. Schlegel, and G. L. Skibinski, "The effects of PWM voltage source inverters on the mechanical performance of rolling bearings," *IEEE Transactions on Industry Applications*, vol. 33, no. 2, pp. 567–576, 1997.
- [7] V. Särkimäki, "Radio frequency measurement method for detecting bearing currents in induction motors," Lappeenranta University of Technology, 2009.
- [8] N. Ville, P. Antti, and A. Jero, "HF near-field probe for magnitude measurements of EDM bearing currents," in *2014 16th European Conference on Power Electronics and Applications*, 2014.
- [9] A. Muetze, V. Niskanen, and J. Ahola, "On Radio-Frequency-Based Detection of High-Frequency Circulating Bearing Current Flow," *IEEE Transactions on Industry Applications*, vol. 50, no. 4, pp. 2592–2601, 2014.
- [10] J. Kalaiselvi and S. Srinivas, "Bearing current profiles in a 3-phase VSI fed induction motor drive using a simplified measurement approach," in

- 2012 *IEEE International Conference on Power Electronics, Drives and Energy Systems (PEDES)*, 2012.
- [11] R. Ong, J. H. Dymond, R. D. Findlay, and B. Szabados, "Shaft current in AC induction machine. An online monitoring system and prediction rules," *IEEE Transactions on Industry Applications*, vol. 37, no. 4, pp. 1189–1196, 2001.
- [12] W. Fei, "Motor shaft voltages and bearing currents and their reduction in multilevel medium-voltage PWM voltage-source-inverter drive applications," *IEEE Transactions on Industry Applications*, vol. 36, no. 5, pp. 1336–1341, Sep–Oct 2000.
- [13] A. Muetze, "Bearing Currents in Inverter-Fed AC-Motors," PhD, Department of Electrical Engineering and Information Technology, Darmstadt University of Technology, 2004.
- [14] U. T. Shami and H. Akagi, "Experimental Discussions on a Shaft End-to-End Voltage Appearing in an Inverter-Driven Motor," *IEEE Transactions on Power Electronics*, vol. 24, no. 6, pp. 1532–1540, 2009.
- [15] A. Muetze and A. Binder, "Techniques for measurement of parameters related to inverter-induced bearing currents," *IEEE transactions on Industry Applications*, vol. 43, no. 5, pp. 1274–1283, 2007.
- [16] J. Ahola, V. Niskanen, and A. Muetze, "On the role of the shaft end in the radio-frequency emission of discharge bearing currents in induction motors," in *Proceedings of the 2011 14th European Conference on Power Electronics and Applications*, 2011: IEEE, pp. 1–10.
- [17] J. Ahola, V. Särkimäki, A. Muetze, and J. Tamminen, "Radio-frequency-based detection of electrical discharge machining bearing currents," *IET Electric Power Applications*, vol. 5, no. 4, pp. 386–392, Apr 2011.
- [18] A. Muetze, J. Tamminen, and J. Ahola, "Influence of Motor Operating Parameters on Discharge Bearing Current Activity," *IEEE Transactions on Industry Applications*, vol. 47, no. 4, pp. 1767–1777, 2011.
- [19] R. Ong, J. H. Dymond, and R. D. Findlay, "Bearing damage analysis in a large oil-ring-lubricated induction machine," *IEEE Transactions on Industrial Electronics*, vol. 47, no. 5, pp. 1085–1091, 2000.
- [20] B. Szabados, R. D. Findlay, J. H. Dymond, and R. Ong, "Systematic practical approach to the study of bearing damage in a large oil-ring-lubricated induction machine," *IEEE Transactions on Industry Applications*, vol. 36, no. 6, pp. 1715–1724, 2000.
- [21] A. Muetze and A. Binder, "Calculation of Circulating Bearing Currents in Machines of Inverter-Based Drive Systems," *IEEE Transactions on Industrial Electronics*, vol. 54, no. 2, pp. 932–938, 2007.
- [22] A. Muetze and A. Binder, "Calculation of influence of insulated bearings and insulated inner bearing seats on circulating bearing currents in machines of inverter-based drive systems," *IEEE Transactions on Industry Applications*, vol. 42, no. 4, pp. 965–972, 2006.
- [23] V. Niskanen, A. Muetze, and J. Ahola, "Study on Bearing Impedance Properties at Several Hundred Kilohertz for Different Electric Machine Operating Parameters," *IEEE Transactions on Industry Applications*, vol. 50, no. 5, pp. 3438–3447, 2014.
- [24] M. Turzynski and P. J. Chrzan, "Reducing Common-Mode Voltage and Bearing Currents in Quasi-Resonant DC-Link Inverter," *IEEE Transactions on Power Electronics*, vol. 35, no. 9, pp. 9553–9562, 2020.
- [25] D. De Gaetano, W. Zhu, X. Sun, X. Chen, A. Griffio, and G. W. Jewell, "Experimental Ball Bearing Impedance Analysis Under Different Speed and Electrical Conditions," *IEEE Transactions on Dielectrics and Electrical Insulation*, vol. 30, no. 3, pp. 1312–1321, 2023.
- [26] A. Muetze, "On a New Type of Inverter-Induced Bearing Current in Large Drives With One Journal Bearing," *IEEE Transactions on Industry Applications*, vol. 46, no. 1, pp. 240–248, 2010.
- [27] S. Chen, T. A. Lipo, and D. Fitzgerald, "Source of induction motor bearing currents caused by PWM inverters," *IEEE Transactions on Energy Conversion*, vol. 11, no. 1, pp. 25–32, 1996.
- [28] J. M. Erdman, R. J. Kerkman, D. W. Schlegel, and G. L. Skibinski, "Effect of PWM inverters on AC motor bearing currents and shaft voltages," *IEEE Transactions on Industry Applications*, vol. 32, no. 2, pp. 250–259, 1996.
- [29] D. Hyypio, "Mitigation of Bearing Electro-Erosion of Inverter-Fed Motors Through Passive Common-Mode Voltage Suppression," *IEEE Transactions on Industry Applications*, vol. 41, no. 2, pp. 576–583, 2005.
- [30] A. Muetze and A. Binder, "Calculation of Motor Capacitances for Prediction of the Voltage Across the Bearings in Machines of Inverter-Based Drive Systems," *IEEE Transactions on Industry Applications*, vol. 43, no. 3, pp. 665–672, 2007.
- [31] A. Muetze and H. W. Oh, "Application of Static Charge Dissipation to Mitigate Electric Discharge Bearing Currents," *IEEE Transactions on Industry Applications*, vol. 44, no. 1, pp. 135–143, 2008.
- [32] O. Magdun, Y. Gemeinder, and A. Binder, "Investigation of influence of bearing load and bearing temperature on EDM bearing currents," in *2010 IEEE Energy Conversion Congress and Exposition* 2010.
- [33] J.-K. Park, T. R. Wellawatta, Z. Ullah, and J. Hur, "New Equivalent Circuit of the IPM-Type BLDC Motor for Calculation of Shaft Voltage by Considering Electric and Magnetic Fields," *IEEE Transactions on Industry Applications*, vol. 52, no. 5, pp. 3763–3771, 2016.
- [34] C. Shaotang and T. A. Lipo, "Circulating type motor bearing current in inverter drives," *IEEE Industry Applications Magazine*, vol. 4, no. 1, pp. 32–38, 1998.
- [35] M. Jaritz, C. Jaeger, M. Bucher, J. Smajic, D. Vukovic, and S. Blume, "An Improved Model for Circulating Bearing Currents in Inverter-Fed AC Machines," in *2019 IEEE International Conference on Industrial Technology (ICIT)*, 2019.
- [36] O. Magdun and A. Binder, "High-Frequency Induction Machine Modeling for Common Mode Current and Bearing Voltage Calculation," *IEEE Transactions on Industry Applications*, vol. 50, no. 3, pp. 1780–1790, 2014.
- [37] O. Magdun, Y. Gemeinder, and A. Binder, "Rotor impedance of the high frequency circulating bearing current path in inverter-fed AC machines," in *2013 IEEE Energy Conversion Congress and Exposition*, 2013.
- [38] M. T. A. Êvo, A. M. Alzamora, I. O. Zapparoli, and H. D. Paula, "Inverter-Induced Bearing Currents: A Thorough Study of the Cause-and-Effect Chains," *IEEE Industry Applications Magazine*, vol. 29, no. 3, pp. 57–66, 2023.
- [39] T. Plazenet, T. Boileau, C. Caironi, and B. Nahid-Mobarakkeh, "A Comprehensive Study on Shaft Voltages and Bearing Currents in Rotating Machines," *IEEE Transactions on Industry Applications*, vol. 54, no. 4, pp. 3749–3759, 2018.
- [40] R. F. Schiferl and M. J. Melfi, "Bearing current remediation options," *IEEE Industry Applications Magazine*, vol. 10, no. 4, pp. 40–50, 2004.
- [41] P. Han, G. Heins, D. Patterson, M. Thiele, and D. M. Ionel, "Modeling of Bearing Voltage in Electric Machines Based on Electromagnetic FEA and Measured Bearing Capacitance," *IEEE Transactions on Industry Applications*, vol. 57, no. 5, pp. 4765–4775, 2021.
- [42] O. Magdun and A. Binder, "Calculation of roller and ball bearing capacitances and prediction of EDM currents," in *2009 35th Annual Conference of IEEE Industrial Electronics*, 2009: IEEE, pp. 1051–1056.